Biophysical Journal, Volume *114*

Supplemental Information

Selective Interaction of Colistin with Lipid Model Membranes

Fernando G. Dupuy, Isabella Pagano, Kathryn Andenoro, Maria F. Peralta, Yasmene Elhady, Frank Heinrich, and Stephanie Tristram-Nagle

SUPPORTING MATERIAL for

Selective interaction of colistin with lipid model membranes

Fernando G. Dupuy[1,2], Isabella Pagano[1], Kathryn Andenoro[1], Maria F. Peralta[1,3], Yasmene Elhady[1], Frank Heinrich[1,4] and Stephanie Tristram-Nagle[1]

[1]*Biological Physics Group, Physics Department, Carnegie Mellon University, Pittsburgh, PA 15213*
[2]*Instituto de Química Biológica, National University of Tucumán, San Miguel de Tucumán, Argentina*
[3]*Instituto de Investigación Médica M y M Ferreyra, CONICET-National University of Córdoba, Córdoba, Argentina*
[4]*National Institute of Standards and Technology Center for Neutron Research, Gaithersburg, MD 20899*

1. Details of CD spectroscopy

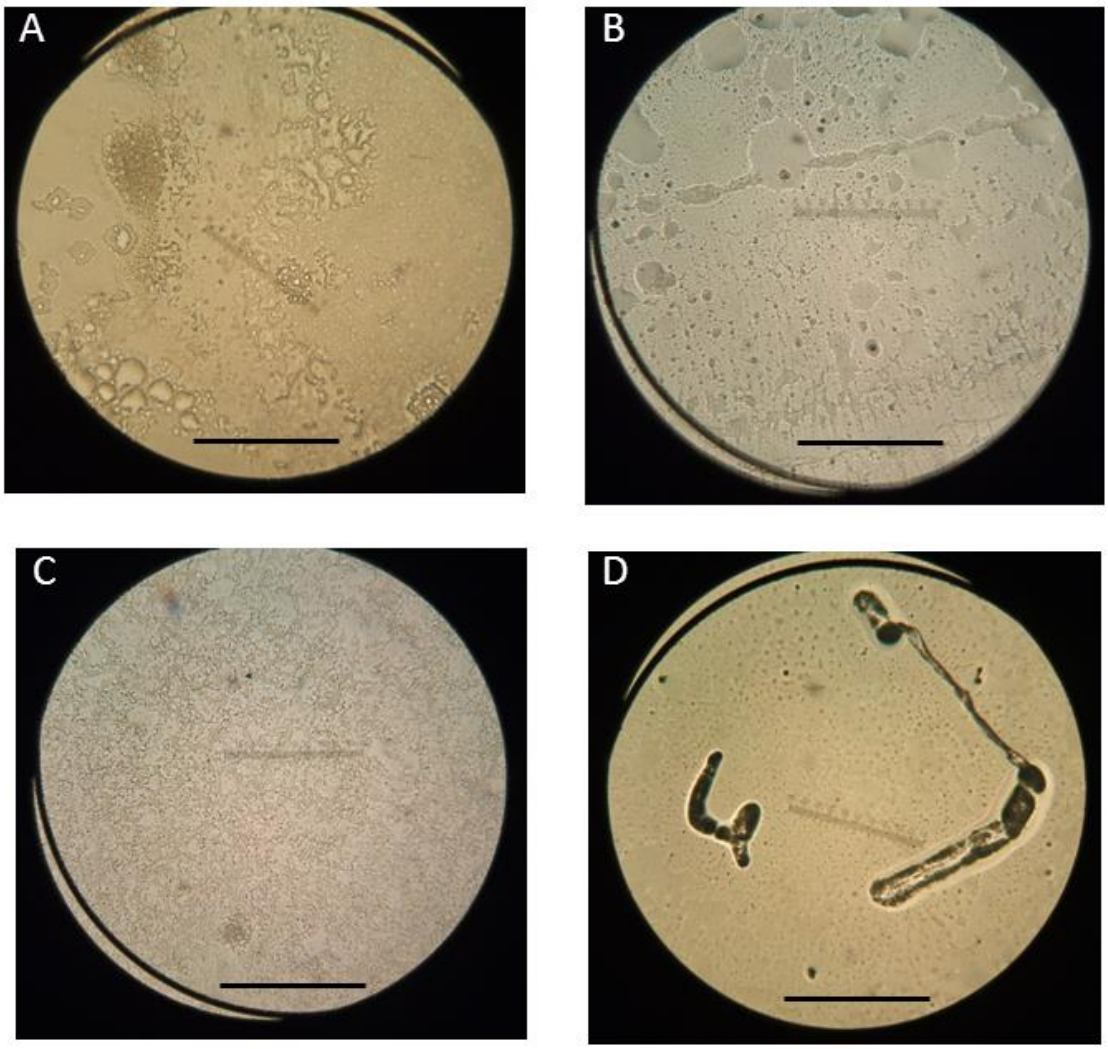

Figure S1. Light microscopy images of thin lipid films on the inner wall of a CD quartz cuvette before hydration. Samples contained colistin mixed with lipid mimics. As shown, samples were not well oriented (homogeneous) and colistin sometimes crystallized out. A. LPS model/colistin, B. G(+) mimic/colistin C. G(-) mimic/colistin D. Eukaryotic (Euk) mimic/colistin. Scale bar represents 500 microns.

Circular Dichroism Results

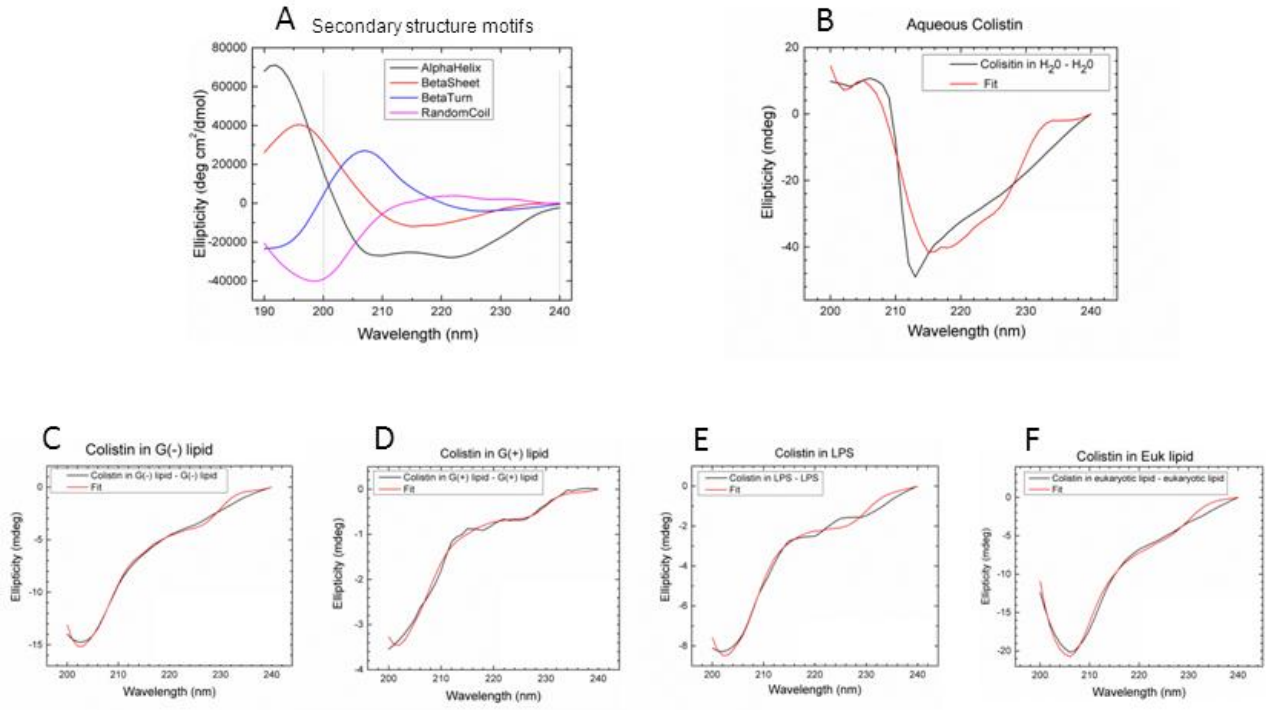

Figure S2. Circular dichroism results. A. Secondary structure motifs from Brahms & Brahms (1), used to fit the CD data between 200 and 240 nm with linear least-squares fitting. B. Colistin in the aqueous phase. C. Colistin in G(-) membrane mimic. D. Colistin in G(+) membrane mimic. E. Colistin in LPS membrane mimic. F. Colistin in Euk membrane mimic. For B-F, data are shown as black lines, fits as red lines. Appropriate background scans were subtracted for each sample. See Table 1 in main paper for motif percentages.

Ellipticity data were collected with a Jasco 715 at 37 ^{o}C in the Center for Molecular Analysis in the Chemistry Department at Carnegie Mellon University. For data analysis, a hyperplane routine supplied by OriginLab Corporation fitted the data over the wavelength range 200 to 240 nm. Hyperplane uses linear least squares to determine the unitless coefficients of the linear combination of the four structural motifs (Fig. S2A) provided by the data set in Ref. (1) using the equation y=A0+(A1*x1)+(A2*x2)+(A3*x3)+(A4*x4). The wavelength range 200 to 240 nm was chosen since it avoids the artefact that the alpha-helix can be fit quite well by the other three motifs if data from 190 to 240 nm are used. Brahms & Brahms (1) used the following reference spectra: beta-turn, poly-$(Ala_2\text{-}Gly_2)_n$. The beta-turn structure is representative of type I and type II, as confirmed by electron microscopy and x-ray diffraction. They refer to an earlier publication (2), that focused on poly-$(Ala_2\text{-}Gly_2)_n$. Alpha-helix was obtained from sperm whale myoglobin in 0.1M NaF pH 7, beta-pleated sheet, poly(lys+-Leu-Lys+-Leu) in 0.5 M NaF at pH 7, and random coil, poly(Pro-Lys+-Leu-Lys+-Leu) in water. The motifs were hand-digitized by Dr. Norma Greenfield from Ref. (1) and placed on this WEBsite: http://rwjms.rutgers.edu/research/cdf/experimental/other.html, where they were retrieved and used in this work. The concentrations of protein used in Ref. (1) are similar to those in this work. The Brahms & Brahms data set was found to be in good agreement with the Reed & Reed data set (3).

2. Details of LAXS data collection and analysis

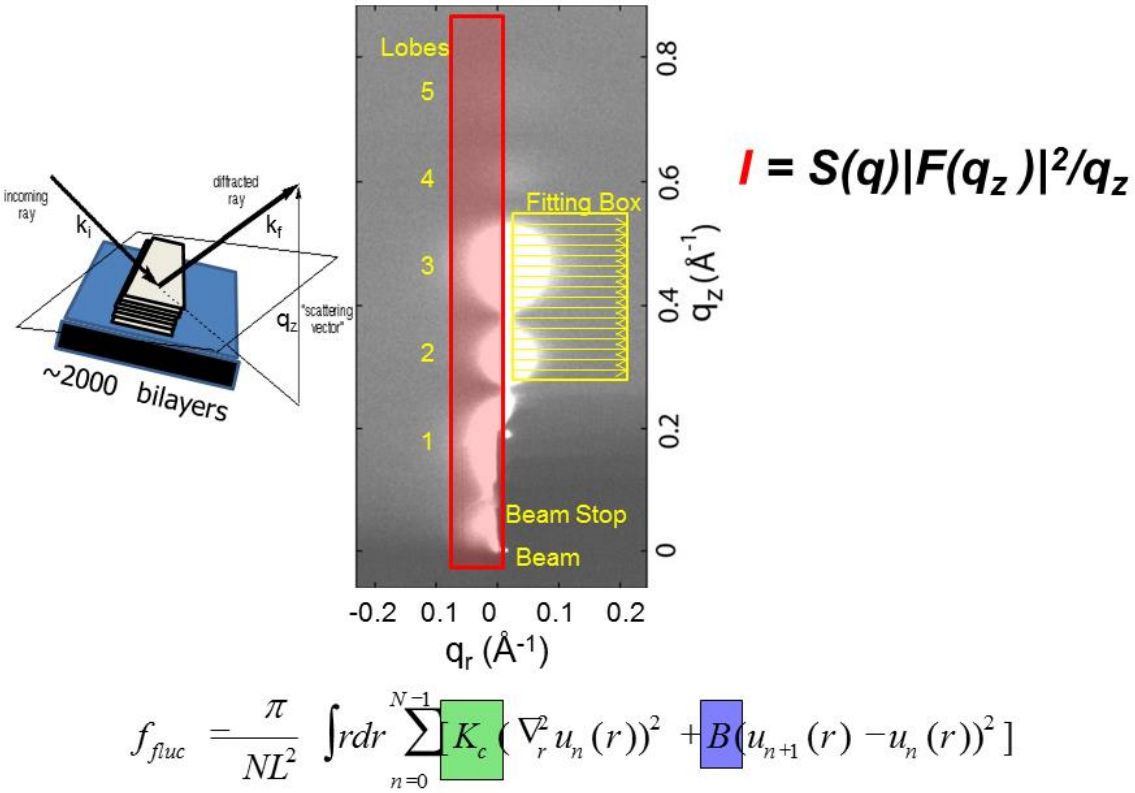

Figure S3. LAXS data collection and analysis. (Figure modified from Ref. (4)).

A stack of ~1800 bilayers on a silicon wafer is hydrated within a hydration chamber (5) (not shown), which causes membrane fluctuations near the fully hydrated condition (6, 7). The wafer is rotated from -1.6 to 7 degrees during the data collection to equally sample all scattered X-rays (30 sec dezingered scans at CHESS or 10 or 20 minute dezingered scans at CMU). Due to the fluctuations, large, nearly spherical "lobes" of diffuse X-ray scattering are produced (numbered in Fig. S3). These fluctuations are quantitated by measuring the fall-off in lobe intensity in the q_r direction in the yellow fitting box shown (4). The fitting procedure is a non-linear least squares fit that uses liquid crystal theory and requires our proprietary software, NFIT. For this work, we used NFIT12.0.5. Usually 30 iterations are required for convergence. By fitting to the free energy functional (equation at bottom of Fig. S3), the structure factor S(q), the bending modulus K_C and the compression modulus B are obtained. Subsequently, these parameters are fixed and the fit is carried out one additional time, fitting the area under the red slice. The result is the form factor, $F(q_z)$, obtained from the corrected scattering intensity (equation on the right in Fig. S3). q_z in this equation is the Lorentz polarization factor. The form factor obtained is then used to fit via the Fourier transform to a model of an electron density profile that uses Gaussians and error functions for the various membrane components. The computer program that carries out this fitting was written by Dr. Norbert Kučerka and is called the Scattering Density Profile (SDP) method (8). One important input to the SDP program is the lipid molecular volume, which is measured as described in Materials and Methods. Densities were measured for the individual membrane mimics and for colistin and appear in Table S1. When electrons are counted, then the Y-axis can be expressed as absolute electron density (e/Å^3).

The headgroup molecular volume is estimated by adding fractional volumes of a PC lipid (9), a PE lipid (10), a PG lipid(11), a TOCL lipid(12), Lipid A(13) and components (10) (see Table S1). The constraints used in the SDP fitting were the Gaussian width of the methyl trough (2-5 Å) and the distance between the carbonyl group position and the hydrocarbon edge (D_C) (1.3 Å). The SDP program yields many structural parameters, including bilayer thickness (D_{HH}, $2D_C$) and area/lipid A_L.

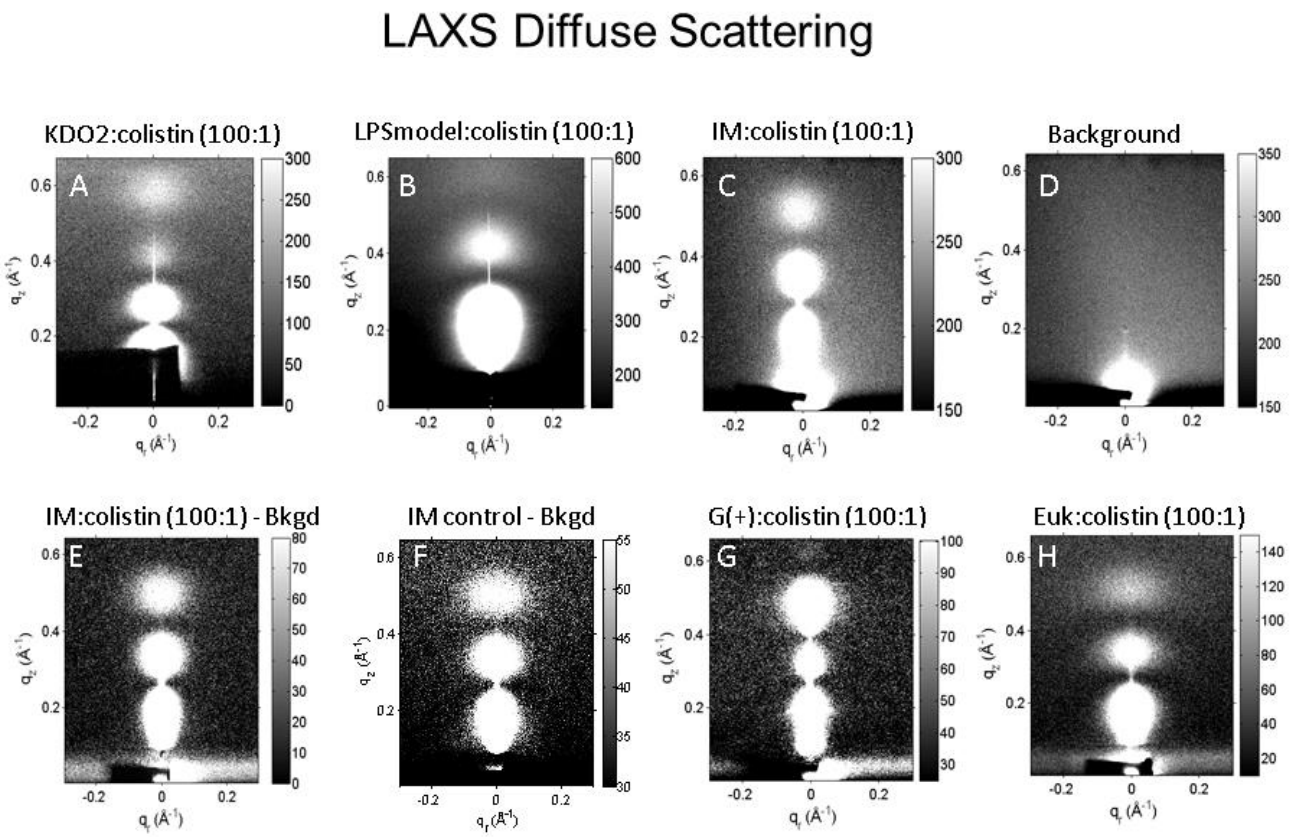

Figure S4. LAXS data collected at 55 ºC at CHESS (A), 37 ºC at CHESS (B) and 37 ºC at CMU (C-H) of membrane mimics with 100:1 lipid:colistin molar ratio. A. KDO2, B. LPS model, C. G(-) IM, D. typical background scan, E. IM – background, F. IM control (no colistin) – background, G. G(+) membrane, H. Euk model. In A, the beam stop (dark rectangle) covers the beam and the first two lamellar orders, while in B-H, the beamstop covers only the beam near the bottom center of each image. The thin, white vertical line in A and B is the X-ray reflectivity from the underlying silicon wafer. Greyscale has been chosen to highlight the diffuse scatter in order to compare samples. All of these samples were fully hydrated as judged by the fact that the D-spacings were either very large (sample is unbinding) or had reached the largest value. The D-spacings for these samples are: A. 144 Å, B. 230 Å, C. 240 Å, E. 240 Å, F. 124 Å, G. 116 Å, H. 67 Å.

Fig. S4 shows typical raw LAXS data from oriented, fully-hydrated stacks of membrane mimics containing colistin. The concentration of lipid:peptide molar ratio (100:1) was chosen for this comparison. For data analysis, backgrounds were first subtracted and the images were symmetrized. An example of a background file is also shown in S4D. The background file was collected by setting the angle of X-ray incidence α = -2.4 degrees. At this angle, the data result from all extraneous scatter from the chamber including the beam overflowing the beamstop. Two examples of files with background subtracted are S4E and S4F. An image of a control sample (S4F), G(-) IM without added colistin, is shown for comparison. Visually, there is little difference between S4E and S4F, but their K_C values are different.

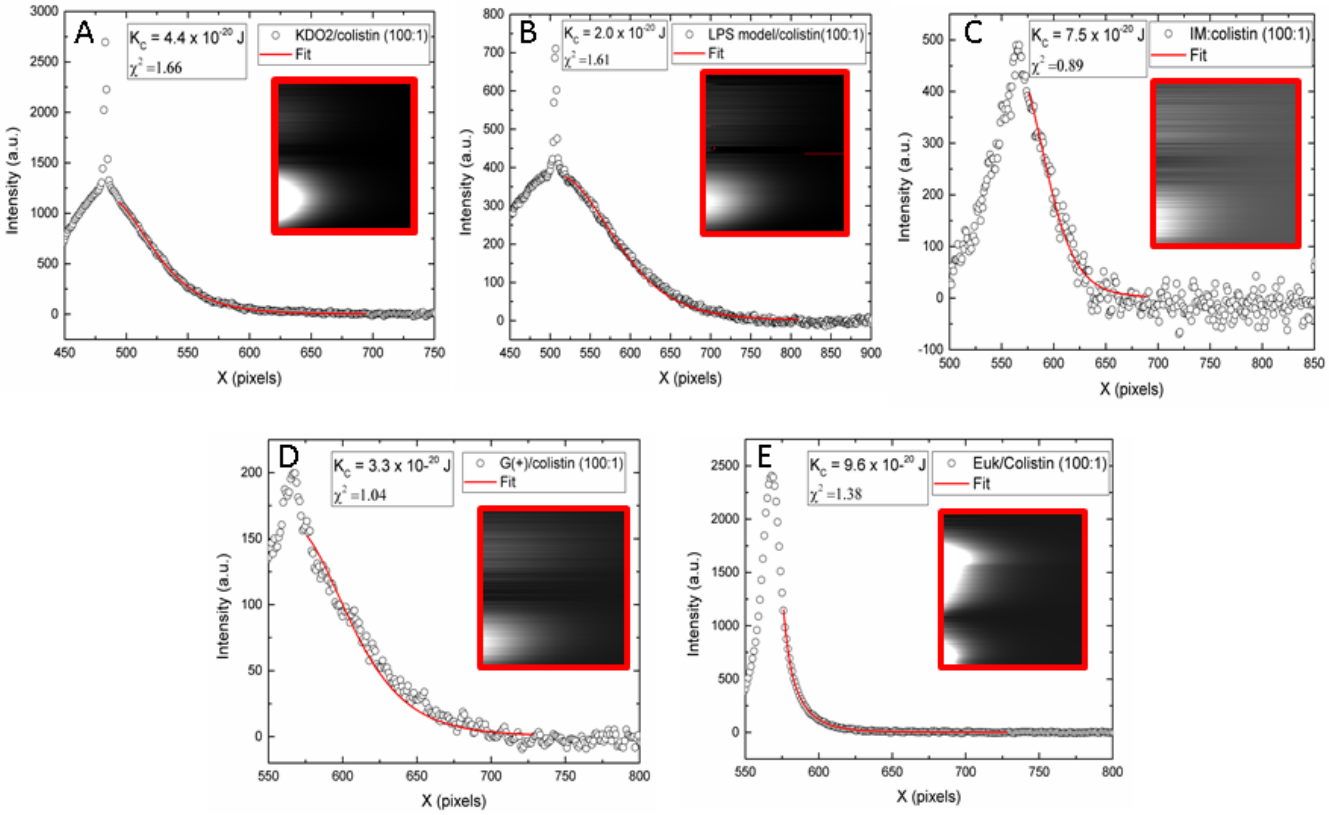

Figure S5. Fits to the liquid crystal diffuse scattering theory shown in Fig. 3 for the five samples in Fig. 4. A. KDO2/colistin (100:1), B. LPS model/colistin (100:1), C. IM:colistin (100:1), D. G(+)/colistin (100:1), E. Euk/colistin (100:1). The 2D images in the red boxes are the fits to the X-ray data in the fitting box shown in Fig. S3. The black open circles result from taking a q_r slice (width 20) at the same position as the highest intensity in the fitted boxes above (red outline). The fits to the data are shown as red lines, which overlay the intensity data fairly well. The chi-square, or goodness of fit, is shown in the legends on the graphs. These fits are typical of most of the data in this study.

Table S1. Volumes of membrane mimic controls and resulting area/lipid A_L.

Sample	**V_L (Å^3)**	**V_{HG} (Å^3)**	**A_L (Å^2)**
KDO2	3420[a]	1371[a]	169
LPS model	3705[a]	1686[a]	223
G(-) IM	1194	259	63.1
Eukaryotic	1108[b]	318	55.2[c]
G(+)	1213	274	66.3
Colistin (aqueous)	1573		

[a]These volumes were calculated based on LipidA volume from MD simulation (13) plus additional component groups with known volumes (10, 14).
[b]Includes cholesterol. [c]Lipid area (no cholesterol).

3. Details of WAXS data collection and analysis

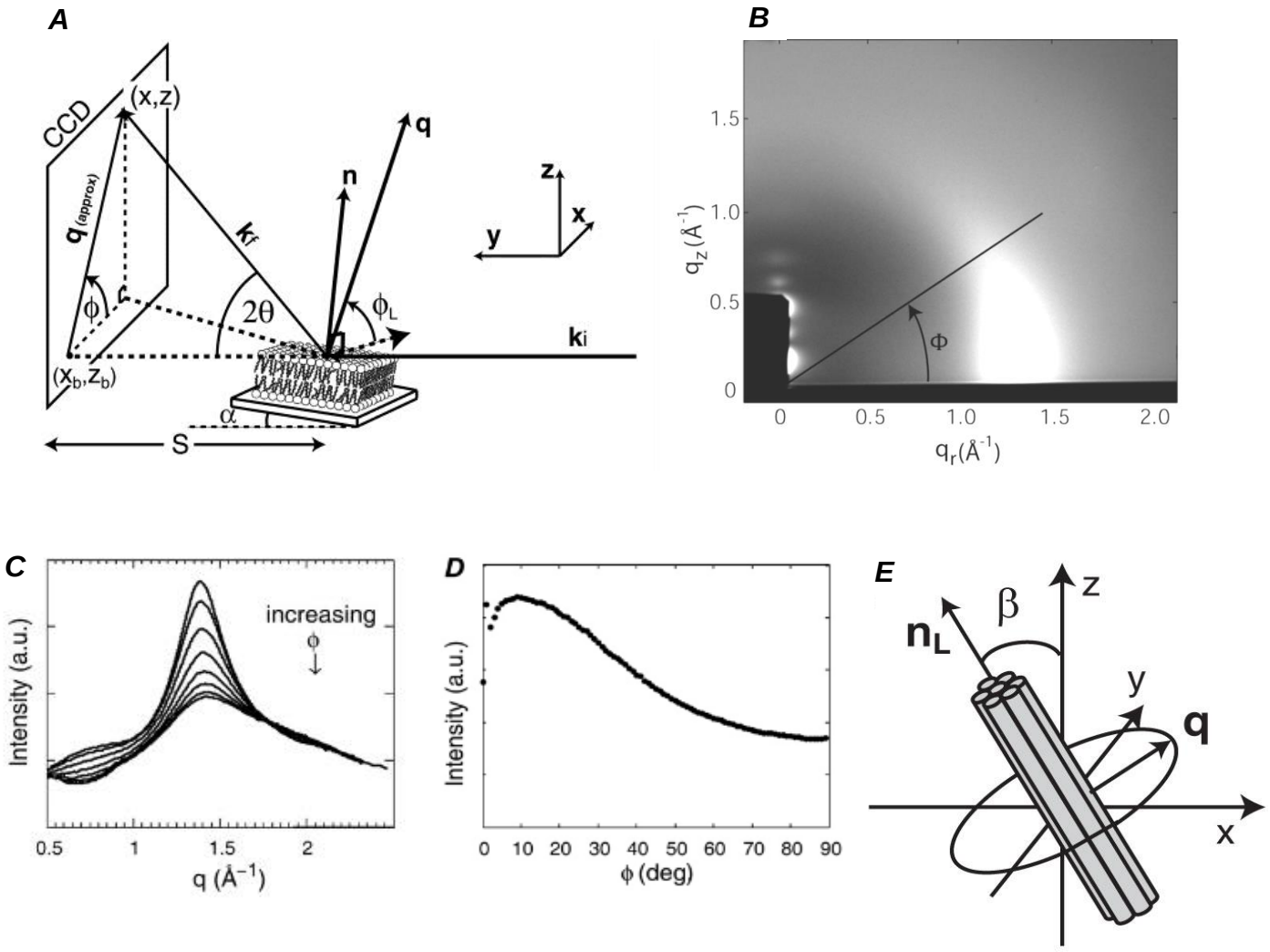

Figure S6. WAXS data collection and analysis. A. Scattering geometry, B. WAXS scattering from a well-ordered sample with background subtracted, C. WAXS intensity as a function of φ angle in 10 degree increments starting at the equator, D. Continuous WAXS intensity as a function of φ angle integrated from 1.2 to 2.2 Å^{-1} in q_r, E. Chain scattering model used to fit to WAXS intensity in D., F. Equation for determination of S_{xray}. Figure adapted from Mills et al. Ref. (15).

In order to obtain WAXS data, the same sample that was hydrated in LAXS is then X-rayed with the CCD detector close to the sample (see S-distances in main paper). Instead of rotating the wafer continuously as in LAXS, two pictures are taken: $\alpha = +0.5$ degrees and $\alpha = -0.5$ degrees. Both are dezingered, 30 second scans (CHESS), or dezingered 10 minute scans (CMU), which are then subtracted from each other. This procedure removes all extraneous scatter due to the mylar chamber windows and shadows. The scattering geometry is shown in Fig. S6A. The chain-chain correlation appears as strong diffuse scatter emanating upwards from the equator in a radial fashion around the φ angle; an example is shown in Fig. S6B. The fall-off in this diffuse intensity around the φ angle yields information about chain order; a steep fall-off, such as shown in Fig. S6B, indicates well-ordered chains, while a more continuous fall-off indicates less ordered chains. In order to carry out the analysis which quantitates the chain orientational order, a sector plot is first made by integrating in 10 degree pie sectors the WAXS intensity starting at the equator. An example of the resulting plot is shown in Fig. S6C. The q_r position of the maximum intensity is used to calculate the interchain d-spacing as $2\pi / q_r = d$. The sector plot is also used to determine the q_r range over which the WAXS intensity will be integrated, which is usually from ~1.2 to ~2.2 $Å^{-1}$. The WAXS intensity is then integrated as a function of φ over the chosen q_r range resulting in the intensity plot shown in Fig. S6D. In the chain scattering model shown in Fig. S6E, long thin rods are locally well aligned along the local director n_L, with orientation described by the angle β. For each grain (group of rods), scattering is permitted only at right angles to n_L. While acyl chains from lipids in the fluid phase are not long cylinders as shown, this model allows the cylinders to tilt (β) to approximate chain disorder. From the fit of the intensity data as a function of φ angle to the liquid crystal theory (15), we obtain S_{xray} using the equation in Fig. S6F, as well as the RMSE (root mean square error), which indicates the goodness of the fit. The order parameter for hydrocarbon chains obtained with WAXS (S_{xray}), although quantitatively lower than S_{CD} from NMR experiments, is able to detect different acyl chain order states in fluid lipid phases as previously shown (15, 16). The fitting is accomplished with a Matlab computer program written by Dr. Thalia Mills and Dr. Gil Toombes. Many more details about this WAXS analysis can be found in Ref. (15) and in the six Supplementary Material sections published in the Biophysical Journal in 2008. Fig. S7 shows WAXS data obtained from the same samples as for the LAXS data in Fig. S4. Fig. S8 shows fits of the theory to the WAXS data shown in Fig. S7.

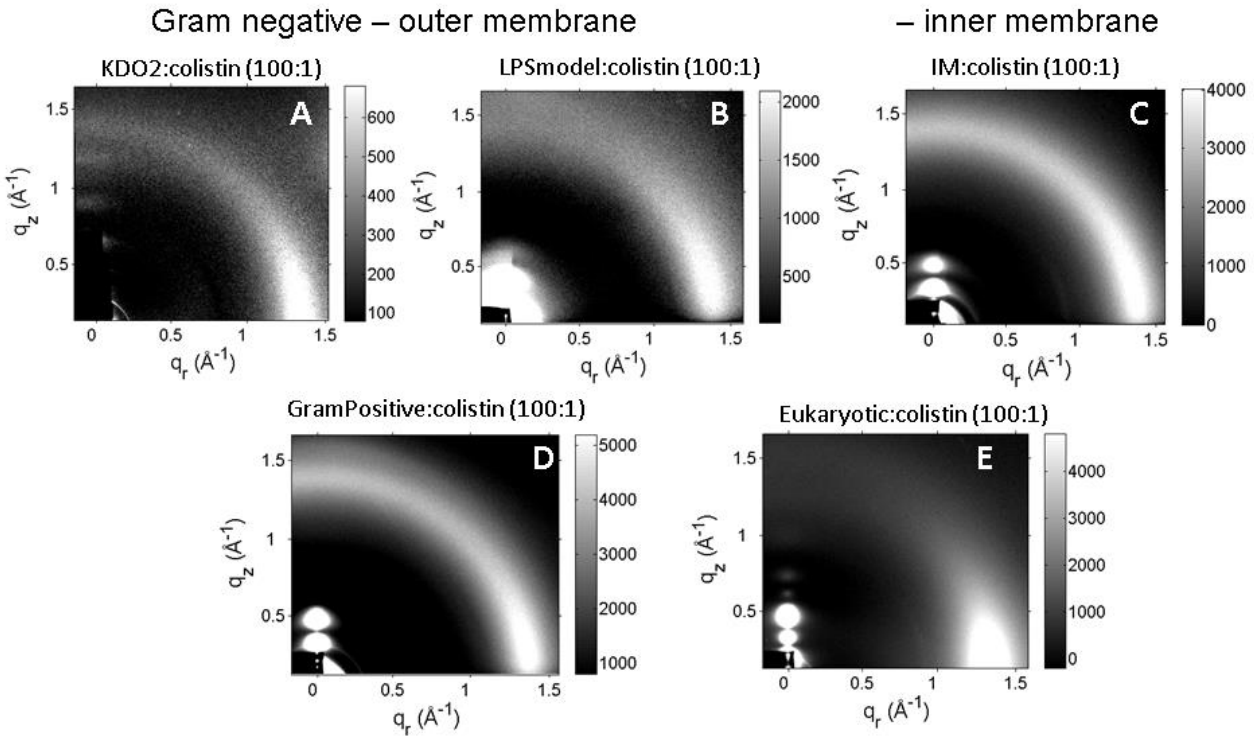

Figure S7. WAXS data collected at 37 ºC at CHESS (B-E) or 55 ºC (A) of membrane mimics at 100:1 lipid:colistin molar ratio. A. KDO2, B. LPS model, C. G(-) IM, D. G(+) membrane, E. Eukaryotic membrane. In A, the beam stop (dark rectangle) covers most of the shrunken LAXS pattern, while in B-E, the beamstop covers one (B) or two (C-E) lamellar orders in the small LAXS pattern near the lower left of the image.

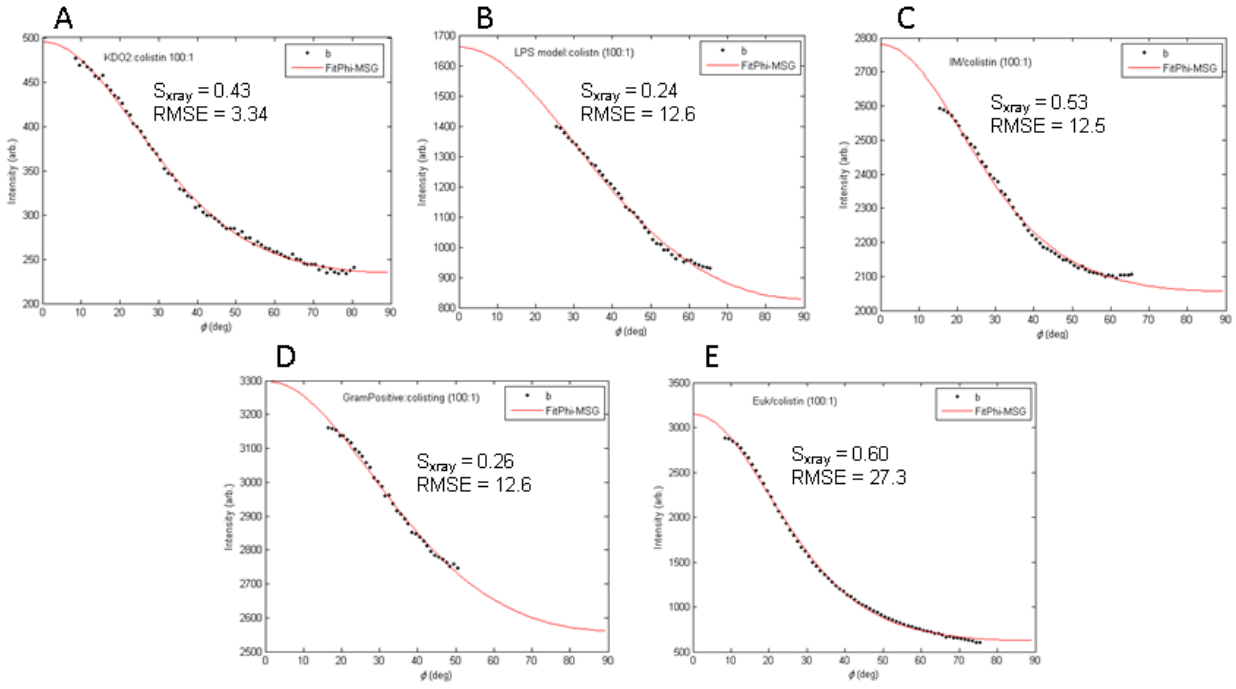

Figure S8. Fits of the WAXS liquid crystal theory shown in Fig. S6E,F to the WAXS data shown in Fig. S7 of membrane mimics at 100:1 lipid:colistin molar ratio. A. KDO2, B. LPS model, C. G(-) IM, D. G(+), E. Eukaryotic.

Details of neutron reflectivity

Details of the vesicle fusion method were described in the main paper. Basically, osmotic pressure causes the small unilamellar vesicles (SUVs) that are attached to the 3" silicon wafer to burst, thus forming the single bilayer shown in Fig. S9A. Rinsing completely removes the salt solution. The resulting bilayer is termed a sparsely tethered bilayer (17) since the tethers from the gold substrate are separated by 2-3 lipid molecules.

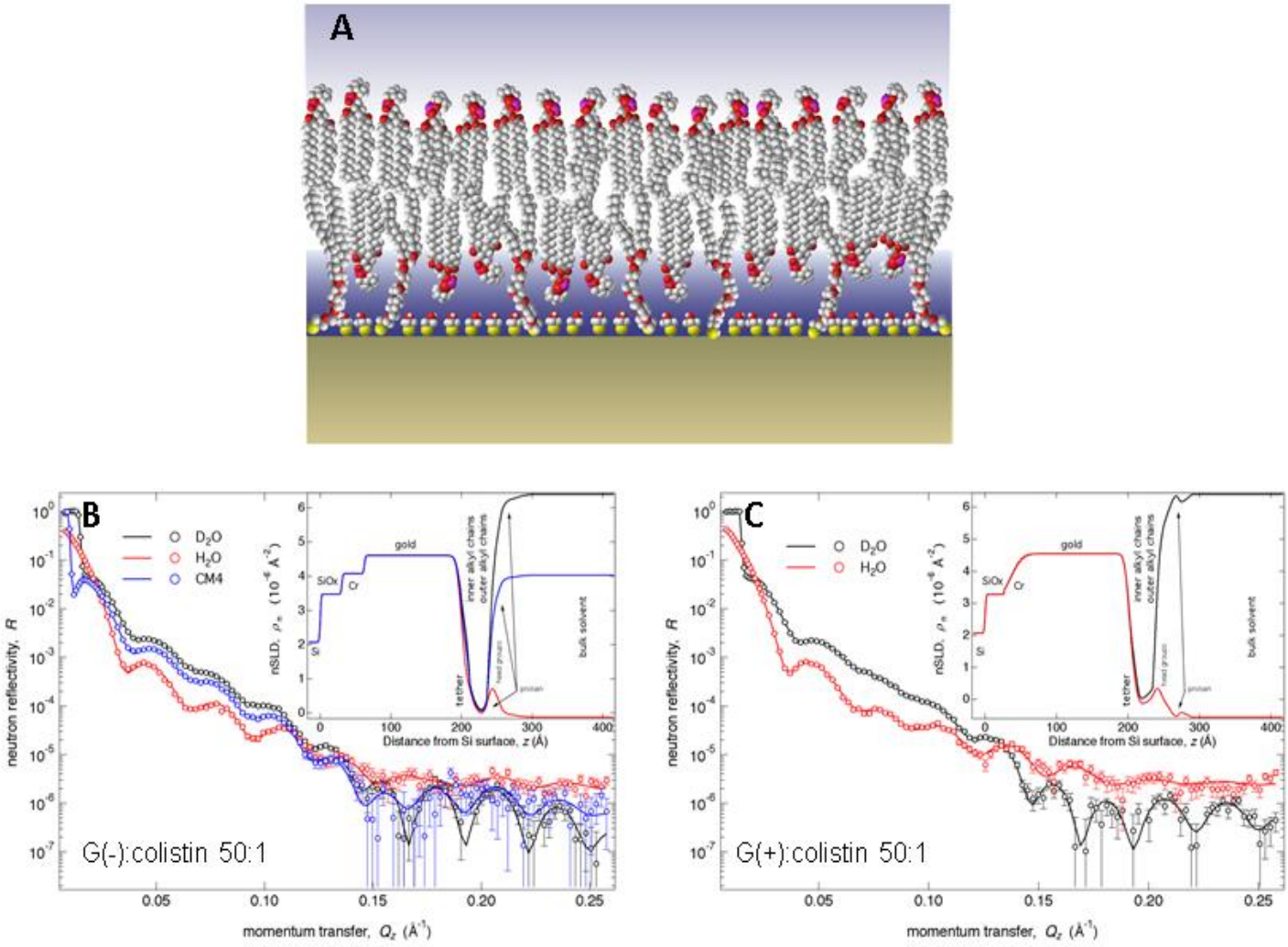

Figure S9. A. Sparsely tethered bilayer without peptide, cartoon adapted from Ref. (18). B. G(-) inner membrane mimic POPE:POPG:TOCL (7:2:1), neutron reflectivity curves (open circles) and best fits (solid lines). Legend indicates contrast solvents used, where CM4 is 67% D_2O and 33% H_2O with nSLD of $4e^{-6}$ $Å^{-2}$. (Inset: Best fit neutron scattering length density profile). C. G(+) membrane mimic POPG:POPE:DOTAP:TOCL (6:1.5:1.5:1), neutron reflectivity curves at two solvent contrasts and corresponding profile in inset. Both samples contained 50:1 lipid:colistin molar ratios.

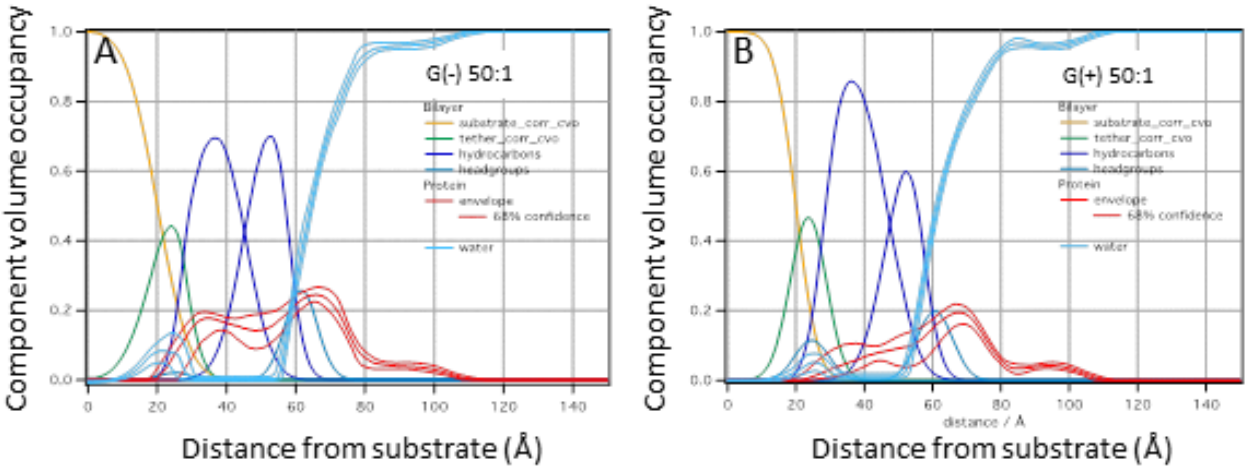

Figure S10. Component volume occupancy vs. distance from substrate of A. G(-) inner membrane and B. G(+) membrane mimics with 50:1 lipid:colistin molar ratio. The 1D-structural profile along the lipid bilayer normal was modeled using a composition space model (19). Median bilayer distributions and median protein profile with 68% confidence limits are shown. These data are also shown in a different format in Fig. 4 in the main paper.

Table S2. Fitting parameters for G(-) membrane mimic with colistin (50:1 molar ratio).

Parameter	Median ± 68% confidence
Tether thickness	9 ± 1 Å
Average hydrocarbon thickness per lipid leaflet	14 ± 3 Å
Area per lipid, outer leaflet	70 ± 20 Å^2
Bilayer completeness	99 ± 1 %
Amount of membrane-associated protein	10.1 ± 0.8 Å^3/Å^2
Fraction of protein in hydrocarbons	0.43± 0.04
Fraction of protein in outer headgroups	0.21 ± 0.03
Fraction of protein in bulk solvent	0.31 ± 0.03

Table S3. Fitting parameters for G(+) membrane mimic with colistin (50:1 molar ratio).

Parameter	Median ± 68% confidence
Tether thickness	8.5 ± 0.3 Å
Average hydrocarbon thickness per lipid leaflet	14 ± 3 Å
Average area per lipid	80 ± 20 Å^2
Bilayer completeness	99 ± 1 %
Amount of membrane-associated protein	6.7 ± 0.8 Å^3/Å^2
Fraction of protein in hydrocarbons	0.31± 0.06
Fraction of protein in outer headgroups	0.23 ± 0.05
Fraction of protein in bulk solvent	0.45 ± 0.05

Selected median model parameters and 68% confidence limits are shown in Tables S2 and S3.

4. Comparing experimental area/lipid A_L with MD simulation.

It is of interest to compare A_L determined using diffuse scattering methods to A_L determined by MD simulation, where many molecular details are observed. In Table S4, experimental A_L's are compared to A_L's obtained from MD simulations. As shown, there is a wide variability, which could be due to experimental conditions, and duration and parameters of the simulations. Another investigation simulated the binding of the related polymyxin B to both Lipid A and KDO2 bilayers, but A_L's were not published (20). A_L remains a central quantity for comparing simulation to experiment.

Table S4. Comparison of Experimental and Simulated A_L

Reference	A_L ($Å^2$)
X-ray (this work) (KDO2)	169
MD simulation (21) (lipid A)	168
X-ray (22) (LPS)	156
MD simulation (13) (lipid A)	151.5
MD simulation (23) (LPS)	130

SUPPORTING REFERENCES

1. Brahms, S., and J. Brahms. 1980. Determination of protein secondary structure in solution by vacuum ultraviolet circular-dichroism. J Mol Biol 138:149-178.
2. Brahms, S., J. Brahms, G. Spach, and A. Brack. 1977. Identification of beta, beta-turns and unordered conformations in polypeptide-chains by vacuum UV circular-dichroism. P Natl Acad Sci USA 74:3208-3212.
3. Reed, J., and T. A. Reed. 1997. A set of constructed type spectra for the practical estimation of peptide secondary structure from circular dichroism. Anal Biochem 254:36-40.
4. Tristram-Nagle, S., and J. F. Nagle. 2004. Lipid bilayers: thermodynamics, structure, fluctuations, and interactions. Chem Phys Lipids 127:3-14.
5. Kucerka, N., Y. F. Liu, N. J. Chu, H. I. Petrache, S. T. Tristram-Nagle, and J. F. Nagle. 2005. Structure of fully hydrated fluid phase DMPC and DLPC lipid bilayers using X-ray scattering from oriented multilamellar arrays and from unilamellar vesicles. Biophys J 88:2626-2637.
6. Liu, Y. F., and J. F. Nagle. 2004. Diffuse scattering provides material parameters and electron density profiles of biomembranes. Phys Rev E 69:040901(R).
7. Lyatskaya, Y., Y. Liu, S. Tristram-Nagle, J. Katsaras, and J. F. Nagle. 2001. Method for obtaining structure and interactions from oriented lipid bilayers. Physical review. E, Statistical, nonlinear, and soft matter physics 63:011907.
8. Kucerka, N., J. F. Nagle, J. N. Sachs, S. E. Feller, J. Pencer, A. Jackson, and J. Katsaras. 2008. Lipid bilayer structure determined by the simultaneous analysis of neutron and X-ray scattering data. Biophys J 95:2356-2367.
9. Tristram-Nagle, S., Y. F. Liu, J. Legleiter, and J. F. Nagle. 2002. Structure of gel phase DMPC determined by X-ray diffraction. Biophys J 83:3324-3335.
10. Nagle, J. F., and S. Tristram-Nagle. 2000. Structure of lipid bilayers. Bba-Rev Biomembranes 1469:159-195.
11. Pan, J. J., F. A. Heberle, S. Tristram-Nagle, M. Szymanski, M. Koepfinger, J. Katsaras, and N. Kucerka. 2012. Molecular structures of fluid phase phosphatidylglycerol bilayers as determined by small angle neutron and X-ray scattering. Bba-Biomembranes 1818:2135-2148.
12. Boscia, A. L., B. W. Treece, D. Mohammadyani, J. Klein-Seetharaman, A. R. Braun, T. A. Wassenaar, B. Klosgen, and S. Tristram-Nagle. 2014. X-ray structure, thermodynamics, elastic properties and MD simulations of cardiolipin/dimyristoylphosphatidylcholine mixed membranes. Chem Phys Lipids 178:1-10.
13. Murzyn, K., and M. Pasenkiewicz-Gierula. 2015. Structural properties of the water/membrane interface of a bilayer built of the E. coli lipid A. J Phys Chem B 119:5846-5856.
14. Molecular Modeling Pro
15. Mills, T. T., G. E. S. Toombes, S. Tristram-Nagle, D. M. Smilgies, G. W. Feigenson, and J. F. Nagle. 2008. Order parameters and areas in fluid-phase oriented lipid membranes using wide angle x-ray scattering. Biophys J 95:669-681.
16. Mills, T. T., S. Tristram-Nagle, F. A. Heberle, N. F. Morales, J. Zhao, J. Wu, G. E. S. Toombes, J. F. Nagle, and G. W. Feigenson. 2008. Liquid-liquid domains in bilayers detected by wide angle x-ray scattering. Biophys J 95:682-690.

17. Barros, M., F. Heinrich, S. A. Datta, A. Rein, I. Karageorgos, H. Nanda, and M. Lösche. 2016. Membrane Binding of HIV-1 Matrix Protein: Dependence on Bilayer Composition and Protein Lipidation. Journal of virology 90:4544-4555.
18. McGillivray, D. J., G. Valincius, D. J. Vanderah, W. Febo-Ayala, J. T. Woodward, F. Heinrich, J. J. Kasianowicz, and M. Lösche. 2007. Molecular-scale structural and functional characterization of sparsely tethered bilayer lipid membranes. Biointerphases 2:21-33.
19. Heinrich, F., and M. Lösche. 2014. Zooming in on disordered systems: Neutron reflection studies of proteins associated with fluid membranes. Bba-Biomembranes 1838:2341-2349.
20. Berglund, N. A., T. J. Piggot, D. Jefferies, R. B. Sessions, P. J. Bond, and S. Khalid. 2015. Interaction of the antimicrobial peptide polymyxin B1 with both membranes of E. coli: a molecular dynamics study. PLoS computational biology 11:e1004180.
21. Wu, E. L., O. Engstrom, S. Jo, D. Stuhlsatz, M. S. Yeom, J. B. Klauda, G. Widmalm, and W. Im. 2013. Molecular dynamics and NMR spectroscopy studies of E. coli lipopolysaccharide structure and dynamics. Biophys J 105:1444-1455.
22. Snyder, S., D. Kim, and T. J. McIntosh. 1999. Lipopolysaccharide bilayer structure: effect of chemotype, core mutations, divalent cations, and temperature. Biochemistry-Us 38:10758-10767.
23. Soares, T. A., Straatsma, T.P. 2008. Assessment of the convergence of molecular dynamics simulations of lipopolysaccharide membranes. Molecular Simulations 34:295-307.